Journal of Crystal Growth 371 (2013) 107–111

Contents lists available at SciVerse ScienceDirect

Journal of Crystal Growth

journal homepage: www.elsevier.com/locate/jcrysgro

In-situ study on growth units of $Ba_2Mg(B_3O_6)_2$ crystal

X.S. Lv [a], Y.L. Sun [a], X.L. Tang [a], S.M. Wan [a,*], Q.L. Zhang [a], J.L. You [b], S.T. Yin [a]

[a] Anhui Key Laboratory for Photonic Devices and Materials, Anhui Institute of Optics and Fine Mechanics, Chinese Academy of Sciences, Hefei 230031, PR China

[b] School of Material Science and Engineering, Shanghai University, Shanghai 200072, PR China

ARTICLE INFO

Article history:
Received 2 November 2012
Received in revised form
2 February 2013
Accepted 17 February 2013
Communicated by S. Uda
Available online 21 February 2013

Keywords:
A1. Crystal morphology
A1. Growth units
A1. High-temperature Raman spectroscopy
A2. Growth from melt
B1. Borates

ABSTRACT

BMBO ($Ba_2Mg(B_3O_6)_2$ crystal) is an excellent birefringent crystal and a potential stimulated Raman scattering (SRS) crystal. In this paper, high temperature Raman spectroscopy was used to *in-situ* study the melt structure near a BMBO crystal–melt interface. $[B_3O_6]^{3-}$ groups were found in this region. The result reveals that both of Ba–O bonds and Mg–O bonds are the weak bonds in the BMBO crystal structure. During the melting process, the crystal structure broke into Ba^{2+} ions, Mg^{2+} ions and $[B_3O_6]^{3-}$ groups. Our experimental results confirmed that the well-developed faces of BMBO crystals are the (001), (101) and (012) faces. Based on attachment energy theory, the crystal growth habit was discussed. The (001) (101) and (012) crystal faces linked by the weak Ba–O bonds and Mg–O bonds have smaller attachment energies and slower growth rates, and thus present in the final morphology. The (012) crystal face has a multi-terrace structure, which suggests that BMBO crystal grows with a layer-by-layer mode.

1. Introduction

$Ba_2Mg(B_3O_6)_2$ crystal (BMBO) was firstly reported by Liebertz et al. in 1984 [1]. Recently, Li et al. obtained a BMBO crystal by spontaneous nucleation; its structure was also determined in their study [2]. The structure of BMBO crystal is isotopic to that of α-BBO (high temperature phase BaB_2O_4). It crystallizes in the trigonal space group $R\bar{3}$ (no. 148) with $a=7.094(5)$ Å, $c=16.721(15)$ Å and $Z=3$. The basic structural units are Ba^{2+} ions, Mg^{2+} ions and $[B_3O_6]^{3-}$ planar six-membered rings. The rings are parallel to each other, forming the $[B_3O_6]^{3-}$ layers perpendicular to the c-axis. Ba^{2+} ions and Mg^{2+} ions alternately locate between two $[B_3O_6]^{3-}$ layers. BMBO crystal is an excellent uniaxial crystal with large birefringences (from 0.0914 to 0.1455 in the range of 2325–253.7 nm), wide transparency range (178–3000 nm) and good physicochemical stability. The crystal can be applied to produce various prism, polarizer, beam displacement and beam splitter, especially those used in deep ultraviolet region [2]. We have studied the spontaneous Raman spectrum of BMBO crystal and found the crystal also is a potential stimulated Raman scattering (SRS) crystal and expected to produce wavelength-specific lasers applied in remote sensing and medical treatment [3,4].

BMBO crystal does not undergo phase transformation on heating and melts congruently at 1002 °C. Hence, the crystal can be grown by the Czochralski or the Kyropoulos method. Our experiments showed that the crystal growth rate along the c-axis direction is lower than other directions by the Kyropoulos method, which makes the growth of large-sized BMBO crystals difficult. The crystal growth mechanism can help us to understand the crystal growth habit. It is well known that crystal growth occurs at crystal–melt interfaces; the melt structure near a crystal–melt interface plays a crucial role in the study of the crystal growth mechanism. However, experimental investigation on the melt structure in this region is very difficult due to the lack of a suitable high-temperature probing technique. Compared with other structural analysis methods, high temperature Raman spectroscopy has the advantages of *in-situ* observations, microanalysis and high temperature measurements, and has been used to *in-situ* investigate the structures of silicate melts and borate melts [5–8]; with the applications of time- and spatial-resolved techniques and UV light sources, its signal-to-noise ratio has been enhanced enormously [9–11]. Our recent works have proved that high temperature Raman spectroscopy is a powerful and convenient tool to *in-situ* study crystal growth mechanisms under high-temperature conditions [12–14]. In this paper, we used this technique to study the growth units of BMBO crystal, and explained its growth habit.

2. Experimental

The experimental system used in this study consists of two parts: a homemade micro-furnace and a high temperature Raman spectrometer (Jobin Y'von LabRAM HR800). The structure of the homemade micro-furnace has been described in detail in our

* Correspondence to: Anhui Institute of Optics and Fine Mechanics, Chinese Academy of Sciences, 350 Shushanhu Road, Hefei 230031, PR China. Tel./fax: +86 551 5591054.
E-mail address: smwan@aiofm.ac.cn (S.M. Wan).

0022-0248/$ - see front matter © 2013 Elsevier B.V. All rights reserved.
http://dx.doi.org/10.1016/j.jcrysgro.2013.02.017

previous work [12]. The BMBO crystals used in this study were grown from $Ba_2Mg(B_3O_6)_2$ melts by the Kyropoulos method. The BMBO crystal was cut into slices with a size of $10 \times 5 \times 1\ mm^3$. One such slice was placed into a platinum boat which was mounted in the center of the micro-furnace. The heating system provided a horizontal temperature gradient in the boat. By carefully controlling the temperature, the BMBO crystal melted on the hot side. After that, the temperature was slowly decreased to allow the crystal to grow gradually on the hot side and consequently a steady crystal–melt interface was produced. Unpolarized Raman spectra of the crystal and the melt were collected at different positions near the crystal–melt interface. All the Raman spectra were recorded with a backscattering configuration. The excitation source was a 355 nm line of a Q-switch pulsed THG-Nd: YAG laser with an average output of 0.8 W. The diameter of the laser beam was less than 2 μm. The laser beam was focused onto the sample through an Olympus BH-2 microscope with the beam direction perpendicular to the (001) crystal face; the Raman scattered light were collected by an intensive charge-coupled device (ICCD). The spectral acquisition, under accumulated mode, was 10 s each time with 10 repetition times. The collecting range of Raman spectra was 200–1800 cm^{-1} with a spectral resolution better than 2 cm^{-1}.

3. Results and discussions

The Raman spectrum of BMBO crystal recorded at room temperature is shown in Fig. 1. The vibrational modes of BMBO crystals can be classified by the method of site group analysis [15]. The crystal has 20 Raman-active vibrational modes, i.e. $10A_g+10E_g$, where E_g is doubly degenerate. In our experimental spectrum, 12 Raman peaks were detected. Two strong Raman peaks located at 646 cm^{-1} and 782 cm^{-1} and four Raman peaks in the range of 1510–1570 cm^{-1} are the characteristic Raman peaks of $[B_3O_6]^{3-}$ rings, and all attributed to the symmetrical vibrations of $[B_3O_6]^{3-}$ rings (Ag mode); their atomic displacements are shown in Fig. 2. The strongest Raman peak at 646 cm^{-1} originates from the breathing vibration of $[B_3O_6]^{3-}$ rings. The Raman peak at 782 cm^{-1} arises from the bending vibration of the intra-ring B–O bonds. The 1513 cm^{-1}, 1524 cm^{-1}, 1540 cm^{-1} and 1560 cm^{-1} peaks are assigned to the same extra-ring B–O stretching vibration of $[B_3O_6]^{3-}$ rings. The boron atoms have two isotopes (^{10}B and ^{11}B), and can form four different metaborate rings, namely $[^{10}B_3O_6]^{3-}$, $[^{10}B_2{}^{11}BO_6]^{3-}$, $[^{10}B^{11}B_2O_6]^{3-}$ and $[^{11}B_3O_6]^{3-}$. As a result, the same extra-ring B–O stretching vibration produces four different Raman peaks due to the isotopic effect [15]. The six Raman peaks all together denote the existence of $[B_3O_6]^{3-}$ rings.

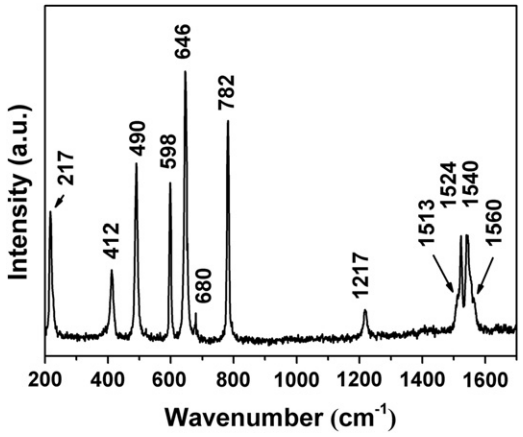

Fig. 1. A typical Raman spectrum of BMBO crystal recorded at room temperature.

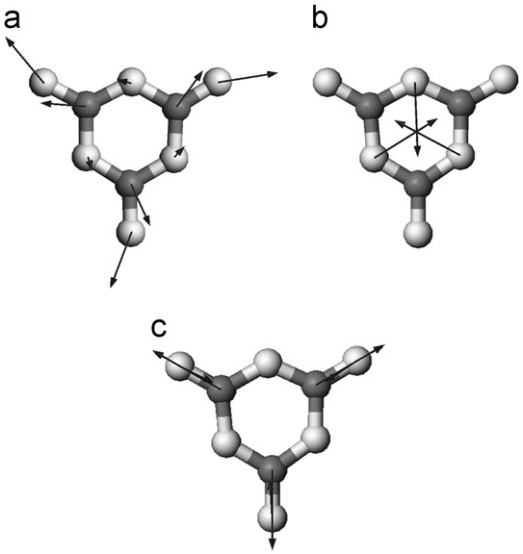

Fig. 2. Atomic displacements of three symmetrical vibrations of $[B_3O_6]^{3-}$ six-membered rings: (a) 646 cm^{-1}, (b) 782 cm^{-1} and (c) 1513 cm^{-1}, 1524 cm^{-1}, 1540 cm^{-1}, 1560 cm^{-1}.

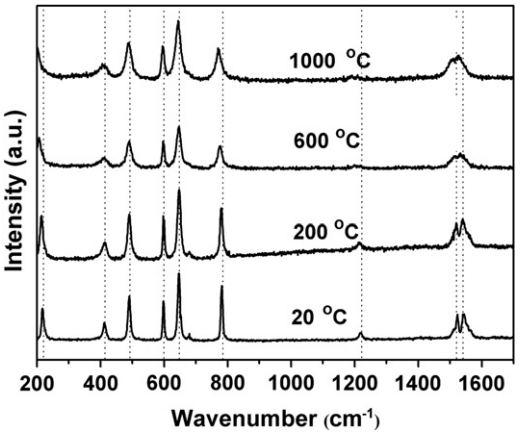

Fig. 3. Raman spectra of BMBO crystal at different temperatures.

Fig. 3 shows the Raman spectra of the BMBO crystal at different temperatures. With temperature increasing, no significant change was found in these spectra except for peak broadening and slight frequency red-shift, which suggests no structural transition occurring in the crystal below 1000 °C.

By carefully controlling the temperature, a stable BMBO crystal–melt interface was obtained. The structures of the crystal and the melt near the interface were studied by high-temperature Raman spectroscopy. The interface morphology and the measuring positions are shown in Fig. 4; the corresponding Raman spectra are shown in Fig. 5 (see the Supplementary materials for more details). At position b (in the crystal, 10 μm from the interface), the main features of the crystal Raman spectrum retain; the high-frequency band in the range of 1300 – 1600 cm^{-1} significantly decreases in frequency. As pointed above, the band originates from the extra-ring B–O stretching vibration of $[B_3O_6]^{3-}$ groups, which implies that the extra-ring B–O bonds weakened when the temperature approached the melting point. We deem that the weakness arises from π-orbital electron transfer. The $[B_3O_6]^{3-}$ ring has a conjugated structure in which the 2p-orbitals of boron atoms overlap with the 2p-orbitals of oxygen atoms to form a conjugated π-orbital, the 2p electrons of

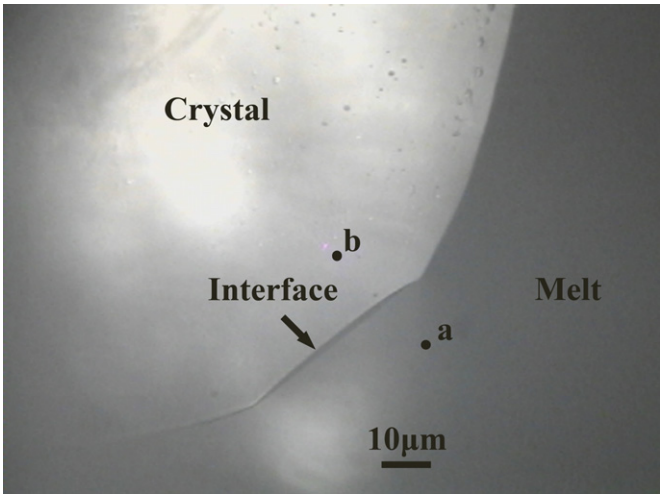

Fig. 4. A typical BMBO crystal–melt interface morphology with the measurement positions. (Position a—in the melt, 10 μm from the interface. Positions b—in the crystal, 10 μm from the interface.)

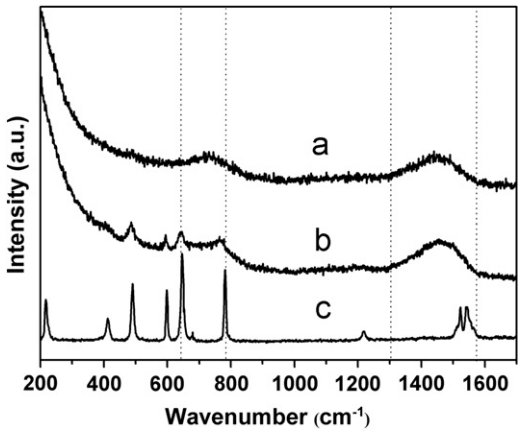

Fig. 5. Raman spectra near crystal–melt interface. (Position a—in the melt, 10 μm from the interface. Positions b—in the crystal, 10 μm from the interface.)

oxygen atoms delocalize over the entire ring [16]. In the BMBO crystal structure, the Ba^{2+} and Mg^{2+} have an electron-withdrawing effect which pulls the π-orbital electrons from the inter-ring B–O bonds to the extra-ring B–O bonds. When the temperature approached to the melting point, the electron-withdrawing effect weakened, and then the π-electrons transferred to the inter-ring B–O bonds from the extra-ring B–O bonds. The electron transfer decreases the force constant of the extra-ring B–O bonds, resulting in the frequency red-shift of the extra-ring B–O stretching vibration. At position a (in the melt, 10 μm from the interface), two wide bands in the range of 400 – 800 cm^{-1} and 1300–1600 cm^{-1} appear. Both of the bands are attributed to the mergence of the characteristic Raman peaks of $[B_3O_6]^{3-}$ rings. For example, the melt peak located around 720 cm^{-1} originates from the broadening and overlapping of the crystal 642 cm^{-1} and 765 cm^{-1} peaks (both of which arise from the symmetrical vibrations of $[B_3O_6]^{3-}$ rings). Based on the results, we conclude that the dominant boron–oxygen structural units in the melt near the BMBO crystal–melt interface are $[B_3O_6]^{3-}$ rings, namely, the basic growth units of BMBO crystal are $[B_3O_6]^{3-}$ rings, Ba^{2+} ions and Mg^{2+} ions. Compared to the crystal structure and the melt structure, we further deduce that Mg–O bonds and Ba–O bonds are the weak bonds in the BMBO crystal structure.

A BMBO single crystal grown by the Kyropoulos method and its morphology are shown in Fig. 6. The well-developed faces of the BMBO crystal are the (001), (101) and (012) faces, which is in agreement with the results reported by Li et al. [2]. Based on the attachment energy theory, we further discussed the crystal growth habit. In 1980, Hartman and Bennema put forward the attachment energy theory based on the PBC (Periodic Bond Chain) model and pointed out that the growth rate of a crystal face Rhkl is proportional to its attachment energy Eatt [17–19]. Namely, the face with a lower attachment energy has a slower growth rate and is more likely to be preserved in the final morphology. Because the face with a low attachment energy is usually linked by weak bonds, we deduce that the face connected by weak bonds is more likely to present in the final morphology. Based on the above analysis of the melt structure near the BMBO crystal–melt interface, we know that Mg–O bonds and Ba–O bonds are the weak bonds in the BMBO crystal structure; hence, the crystal faces connected by Mg–O or Ba–O bonds have low attachment energies and slow growth rates, and are thus more probable to appear in the final crystal morphology. From the BMBO crystal structure, we know that the (001), (101) and (012) crystal faces are all connected by Mg–O bonds or Ba–O bonds (see Fig. 7) and thus the well-developed crystal faces. The Mg^{2+} layers, parallel to the (001) face, have a minimal face density of Mg–O/Ba–O bonds, which leads to the lowest attachment energy along the (001) face as compared to the (101) and the (012) faces. As a result, the (001) face grows most slowly and presents in the final crystal morphology as the largest face.

A micrograph of the (012) face is shown in Fig. 8(a). The surface is characterized by a well-ordered step-terrace array; the direction of the terrace edges are along the a-axis. According to the crystal growth habit, we consider that the (012) face is composed by the (001) terraces (see Fig. 8(b)). The multi-terrace structure indicates that the crystal grows with a layer-by-layer mode [20].

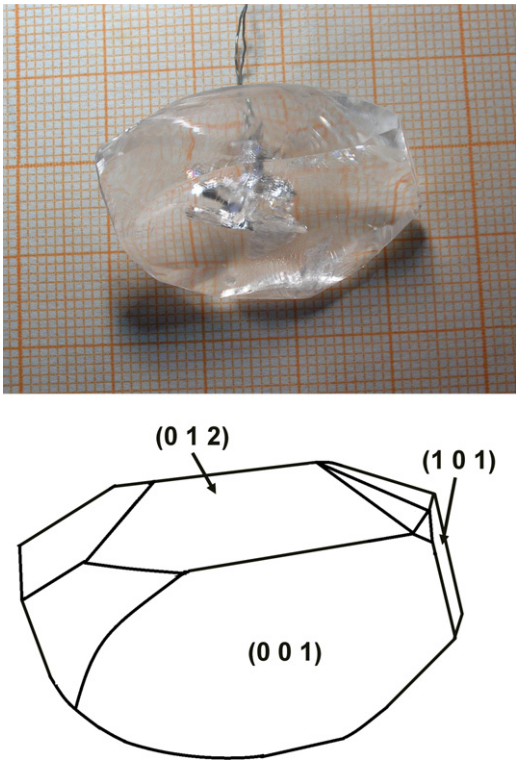

Fig. 6. A picture of a BMBO crystal and its morphology.

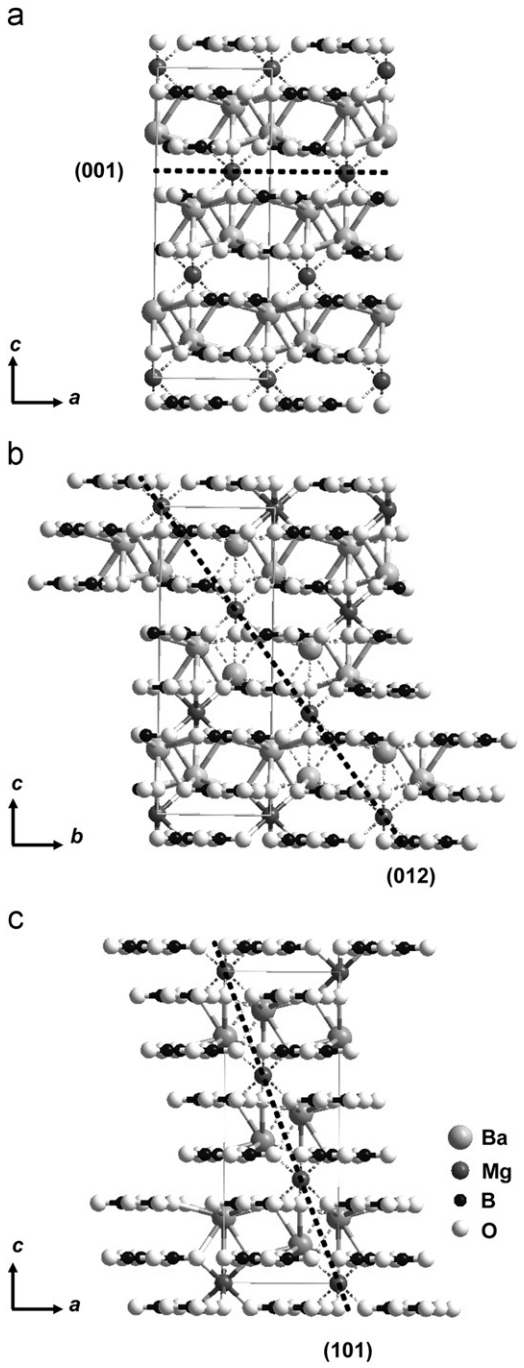

Fig. 7. Packing arrangement of BMBO crystal structure as viewed along (a) the b-axis, (b) the a-axis, and (c) the b-axis.

4. Conclusions

The melt structure near a BMBO crystal–melt interface was studied by high temperature Raman spectroscopy. The results show that the growth units of BMBO crystal are Ba^{2+} ions, Mg^{2+} ions and $[B_3O_6]^{3-}$ six-membered rings. Based on the attachment energy theory and the structural features of BMBO crystal, we discussed the growth habit of BMBO crystal. The growth of BMBO crystal is associated with the formation of Ba–O bonds and Mg–O bonds. The (001), (101) and (012) faces connected by the weak Ba–O bonds and Mg–O bonds have low attachment energies and will present in the final crystal morphology. According to the surface micrograph of the (012) face, a layer-by-layer mechanism was proposed to explain the crystal growth process.

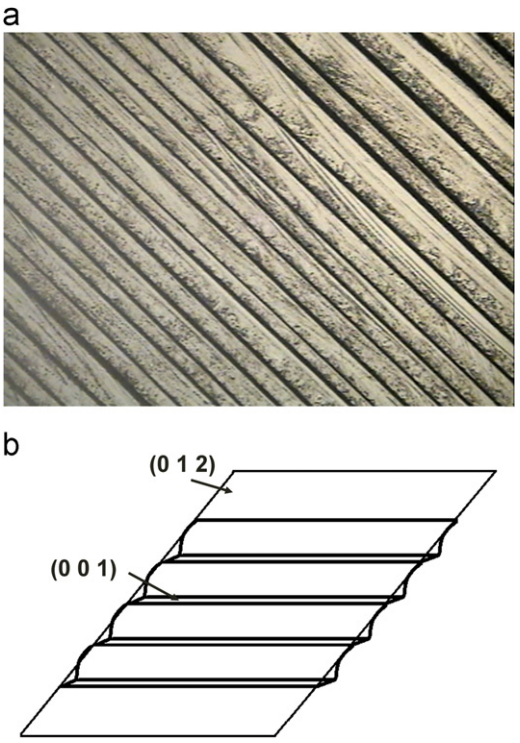

Fig. 8. An 1100 μm × 800 μm micrograph of the (012) face of a BMBO crystal.

Acknowledgment

This work is financially supported by the National Natural Science Foundation of China (Grant no. 50932005) and Open Research Program of Key Laboratory of Functional Crystals and Laser Technology, Technical Institute of Physics and Chemistry, Chinese Academy of Sciences.

Appendix A. Supplementary material

Supplementary materials associated with this article can be found in the online version at http://dx.doi.org/10.1016/j.jcrysgro.2013.02.017.

References

[1] J. Liebertz, R. Fröhlich, Zeitschrift Fur Kristallographie 168 (1984) 293.
[2] R.K. Li, Y.Y. Ma, Crystal Engineering Communications 14 (2012) 5421.
[3] J.H. Hulliger, A.A. Kaminskii, H.J. Eichler, Advanced Functional Materials 11 (2001) 243.
[4] A.D. Greentree, S. Prawer, Nature Photonics 4 (2010) 202.
[5] T. Yano, S. Shibata, T. Maehara, Journal of the American Ceramic Society 89 (2006) 89.
[6] G.S. Henderson, Canadian Mineralogist 43 (2005) 1921.
[7] V.P. Solntsev, A.V. Davydov, V.K. Malinovsky, N.V. Surovtsev, Journal of Crystal Growth 312 (2010) 2962.
[8] N.V. Surovtsev, V.K. Malinovsky, V.P. Solntsev, A.V. Davydov, E.G. Tsvetkov, Journal of Crystal Growth 310 (2008) 3540.
[9] Yu.K. Voron'ko, A.B. Kudryavtsev, V.V. Osiko, A.A. Sobol', High-temperature Raman scattering studies of melt structure and crystallization processes, in: S. Kh., E.B.Lube Bagdasarov (Eds.), Growth of Crystals, Consultant Bureau, New York, 1991, pp. 199–216.
[10] B.O. Mysen, J.D. Frantz, Chemical Geology 96 (1992) 321.
[11] M. Yashima, M. Kakihana, R. Shimidzu, H. Fujimori, M. Yoshimura, Applied Spectroscopy 51 (1997) 1224.

[12] S.M. Wan, X. Zhang, S.J. Zhao, Q.L. Zhang, J.L. You, H. Chen, G.C. Zhang, S.T. Yin, Journal of Applied Crystallography 40 (2007) 725.
[13] S.M. Wan, X. Zhang, S.J. Zhao, Q.L. Zhang, J.L. You, L. Lu, P.Z. Fu, Y.C. Wu, S.T. Yin, Crystal Growth and Design 8 (2008) 412.
[14] D. Wang, S.M. Wan, S.T. Yin, Q.L. Zhang, J.L. You, G.C. Zhang, P.Z. Fu, Crystal Engineering Communications 13 (2011) 5239.
[15] X.S. Lv, Y.L. Sun, J. Han, G.X. Gu, S.M. Wan, M.J. Cheng, S.L. Pan, Q.L. Zhang, Journal of Crystal Growth 363 (2013) 220.
[16] R.H. French, J.W. Ling, F.S. Ohuchi, C.T. Chen, Physical Review B 44 (1991) 8496.
[17] P. Hartman, P. Bennema, Journal of Crystal Growth 49 (1980) 145.
[18] P. Hartman, Journal of Crystal Growth 49 (1980) 157.
[19] P. Hartman, Journal of Crystal Growth 49 (1980) 166.
[20] I.V. Markov, Crystal Growth for Beginners, World Scientific Publishing Co. Pte. Ltd., Singapore, 2003.